The Meteoritical Society

Meteoritics & Planetary Science 59, Nr 8, 1966–1982 (2024)
doi: 10.1111/maps.14109

Neodymium-142 deficits and samarium neutron stratigraphy of C-type asteroid (162173) Ryugu

Zachary A. TORRANO[1]*, Michelle K. JORDAN[1], Timothy D. MOCK[1], Richard W. CARLSON[1], Ikshu GAUTAM[2], Makiko K. HABA[2], Tetsuya YOKOYAMA[2], Yoshinari ABE[3], Jérôme ALÉON[4], Conel ALEXANDER[1], Sachiko AMARI[5,6], Yuri AMELIN[7], Ken-ichi BAJO[8], Martin BIZZARRO[9], Audrey BOUVIER[10], Marc CHAUSSIDON[11], Byeon-Gak CHOI[12], Nicolas DAUPHAS[13], Andrew M. DAVIS[13], Tommaso DI ROCCO[14], Wataru FUJIYA[15], Ryota FUKAI[16], Yuki HIBIYA[17], Hiroshi HIDAKA[18], Hisashi HOMMA[19], Peter HOPPE[20], Gary R. HUSS[21], Kiyohiro ICHIDA[22], Tsuyoshi IIZUKA[23], Trevor IRELAND[24], Akira ISHIKAWA[2], Shoichi ITOH[25], Noriyuki KAWASAKI[8], Noriko T. KITA[26], Koki KITAJIMA[26], Thorsten KLEINE[27], Shintaro KOMATANI[22], Alexander N. KROT[21], Ming-Chang LIU[28], Yuki MASUDA[2], Kevin D. MCKEEGAN[28], Mayu MORITA[22], Kazuko MOTOMURA[29], Frédéric MOYNIER[11], Izumi NAKAI[30], Kazuhide NAGASHIMA[21], Ann NGUYEN[31], Larry NITTLER[32], Morihiko ONOSE[22], Andreas PACK[14], Changkun PARK[33], Laurette PIANI[34], Liping QIN[35], Sara RUSSELL[36], Naoya SAKAMOTO[37], Maria SCHÖNBÄCHLER[38], Lauren TAFLA[29], Haolan TANG[35], Kentaro TERADA[39], Yasuko TERADA[40], Tomohiro USUI[16], Sohei WADA[26], Meenakshi WADHWA[32], Richard J. WALKER[41], Katsuyuki YAMASHITA[42], Qing-Zhu YIN[43], Shigekazu YONEDA[44], Edward D. YOUNG[29], Hiroharu YUI[45], Ai-Cheng ZHANG[46], Tomoki NAKAMURA[47], Hiroshi NARAOKA[48], Takaaki NOGUCHI[25], Ryuji OKAZAKI[48], Kanako SAKAMOTO[16], Hikaru YABUTA[49], Masanao ABE[16], Akiko MIYAZAKI[16], Aiko NAKATO[16], Masahiro NISHIMURA[16], Tatsuaki OKADA[16], Toru YADA[16], Kasumi YOGATA[16], Satoru NAKAZAWA[16], Takanao SAIKI[16], Satoshi TANAKA[16], Fuyuto TERUI[50], Yuichi TSUDA[16], Sei-ichiro WATANABE[18], Makoto YOSHIKAWA[16], Shogo TACHIBANA[51], and Hisayoshi YURIMOTO[26]

[1]Earth and Planets Laboratory, Carnegie Institution for Science, Washington, DC, USA
[2]Department of Earth and Planetary Sciences, Tokyo Institute of Technology, Tokyo, Japan
[3]Graduate School of Engineering Materials Science and Engineering, Tokyo Denki University, Tokyo, Japan
[4]Institut de Minéralogie, de Physique des Matériaux et de Cosmochimie, Sorbonne Université, Museum National d'Histoire Naturelle, CNRS UMR 7590, IRD, Paris, France
[5]McDonnell Center for the Space Sciences and Physics Department, Washington University, St. Louis, Missouri, USA
[6]Geochemical Research Center, The University of Tokyo, Tokyo, Japan
[7]Guangzhou Institute of Geochemistry, Chinese Academy of Sciences, Guangzhou, China
[8]Department of Natural History Sciences, IIL, Hokkaido University, Sapporo, Japan
[9]Centre for Star and Planet Formation, GLOBE Institute, University of Copenhagen, Copenhagen, Denmark
[10]Bayerisches Geoinstitut, Universität Bayreuth, Bayreuth, Germany
[11]Université Paris Cité, Institut de physique du globe de Paris, CNRS, Paris, France
[12]Department of Earth Science Education, Seoul National University, Seoul, Republic of Korea
[13]Department of the Geophysical Sciences, Enrico Fermi Institute, The University of Chicago, Chicago, Illinois, USA
[14]Faculty of Geosciences and Geography, University of Göttingen, Göttingen, Germany
[15]Faculty of Science, Ibaraki University, Mito, Japan
[16]ISAS/JSEC, JAXA, Sagamihara, Japan
[17]General Systems Studies, The University of Tokyo, Tokyo, Japan
[18]Earth and Planetary Sciences, Nagoya University, Nagoya, Japan
[19]Osaka Application Laboratory, SBUWDX, Rigaku Corporation, Osaka, Japan
[20]Max Planck Institute for Chemistry, Mainz, Germany

[21]Hawai'i Institute of Geophysics and Planetology, University of Hawai'i at Mānoa, Honolulu, Hawaii, USA
[22]Analytical Technology, Horiba Techno Service Co., Ltd, Kyoto, Japan
[23]Earth and Planetary Science, The University of Tokyo, Tokyo, Japan
[24]School of Earth and Environmental Sciences, The University of Queensland, St Lucia, Queensland, Australia
[25]Earth and Planetary Sciences, Kyoto University, Kyoto, Japan
[26]Geoscience, University of Wisconsin-Madison, Madison, Wisconsin, USA
[27]Max Planck Institute for Solar System Research, Göttingen, Germany
[28]Earth, Planetary, and Space Sciences, UCLA, Los Angeles, California, USA
[29]Thermal Analysis, Rigaku Corporation, Tokyo, Japan
[30]Applied Chemistry, Tokyo University of Science, Tokyo, Japan
[31]Astromaterials Research and Exploration Science, NASA Johnson Space Center, Houston, Texas, USA
[32]School of Earth and Space Exploration, Arizona State University, Tempe, Arizona, USA
[33]Earth-System Sciences, Korea Polar Research Institute, Incheon, Korea
[34]Centre de Recherches Pétrographiques et Géochimiques, CNRS—Université de Lorraine, Nancy, France
[35]CAS Key Laboratory of Crust-Mantle Materials and Environments, University of Science and Technology of China, School of Earth and Space Sciences, Anhui, China
[36]Department of Earth Sciences, Natural History Museum, London, UK
[37]Isotope Imaging Laboratory, Creative Research Institution, Hokkaido University, Sapporo, Japan
[38]Department of Earth Sciences, ETH Zurich, Institute for Geochemistry and Petrology, Zurich, Switzerland
[39]Earth and Space Science, Osaka University, Osaka, Japan
[40]Spectroscopy and Imaging, Japan Synchrotron Radiation Research Institute, Hyogo, Japan
[41]Geology, University of Maryland, College Park, Maryland, USA
[42]Graduate School of Natural Science and Technology, Okayama University, Okayama, Japan
[43]Earth and Planetary Sciences, University of California, Davis, California, USA
[44]Science and Engineering, National Museum of Nature and Science, Tsukuba, Japan
[45]Chemistry, Tokyo University of Science, Tokyo, Japan
[46]School of Earth Sciences and Engineering, Nanjing University, Nanjing, China
[47]Department of Earth Science, Tohoku University, Sendai, Japan
[48]Department of Earth and Planetary Sciences, Kyushu University, Fukuoka, Japan
[49]Earth and Planetary Systems Science Program, Hiroshima University, Higashi-Hiroshima, Japan
[50]Kanagawa Institute of Technology, Atsugi, Japan
[51]UTokyo Organization for Planetary and Space Science, University of Tokyo, Tokyo, Japan
***Correspondence**
Zachary A. Torrano, Earth and Planets Laboratory, Carnegie Institution for Science, Washington, DC 20015, USA.
Email: ztorrano@carnegiescience.edu

(Received 10 April 2023; revision accepted 24 November 2023)

Abstract–We report Nd and Sm isotopic compositions of four samples of Ryugu returned by the Hayabusa2 mission, including "A" (first touchdown) and "C" (second touchdown) samples, and several carbonaceous chondrites to evaluate potential genetic relationships between Ryugu and known chondrite groups and track the cosmic ray exposure history of Ryugu. We resolved Nd and Sm isotopic anomalies in small (<20 ng Nd and Sm) sample sizes via thermal ionization mass spectrometer using 10^{13} Ω amplifiers. Ryugu samples exhibit resolvable negative μ^{142}Nd values consistent with carbonaceous chondrite values, suggesting that Ryugu is related to the parent bodies of carbonaceous chondrites. Ryugu's negative μ^{149}Sm values are the result of exposure to galactic cosmic rays, as demonstrated by the correlation between $^{150}Sm/^{152}Sm$ and $^{149}Sm/^{152}Sm$ ratios that fall along the expected neutron capture correlation line. The neutron fluence calculated in the "A" samples ($2.75 \pm 1.94 \times 10^{15}$ n cm^{-2}) is slightly higher compared to the "C" samples ($0.95 \pm 2.04 \times 10^{15}$ n cm^{-2}), though overlapping within measurement uncertainty. The Sm results for Ryugu, at this level of precision, thus are consistent with a well-mixed surface layer at least to the depths from which the "A" and "C" samples derive.

INTRODUCTION

Carbonaceous chondrites are primitive undifferentiated meteorites that have been linked to C-type asteroids based on spectral characteristics, but direct comparisons of petrologic, chemical, and isotopic properties in the laboratory were impossible until recently. The JAXA Hayabusa2 spacecraft was launched in 2014 with the goal of collecting samples from the Cb-type near-Earth asteroid (162173) Ryugu and returning them to Earth to study the nature of C-type asteroids and evaluate possible relationships with carbonaceous chondrites. Remote observations of Ryugu from the Hayabusa2 spacecraft revealed that Ryugu appeared darker (Kitazato et al., 2019; Sugita et al., 2019) and more porous (Grott et al., 2019; Okada et al., 2020) than carbonaceous chondrites, but these characteristics may reflect space weathering and impact gardening and reinforce the need for laboratory analyses of returned samples to elucidate the relationship between carbonaceous chondrites and Ryugu.

The Hayabusa2 mission returned a total mass of 5.4 g of material (Tachibana et al., 2022) to Earth in 2020. Subsequent laboratory investigations have studied the petrologic, chemical, and isotopic composition of the returned Ryugu samples. Petrologic analyses demonstrated that Ryugu samples are mixtures of fine- and coarse-grained fragments, with few Ca-Al-rich inclusions (CAIs) or chondrules present (Nakamura et al., 2022). Analyses of bulk elemental abundances revealed no systematic depletions relative to CI chondrites as a function of volatility, unlike other carbonaceous chondrite groups, indicating that Ryugu samples may be related to CI (Ivuna-like) chondrites (Yokoyama et al., 2023). The relationship between Ryugu samples and carbonaceous chondrites, and more specifically CI chondrites, is further supported by Ti and Cr (Yokoyama et al., 2023), Fe (Hopp et al., 2022), Cu and Zn (Paquet et al., 2022), Ca (Moynier et al., 2022), and O (Kawasaki et al., 2022; Yokoyama et al., 2023) isotopic compositions and ^{53}Mn–^{53}Cr dating of aqueous alteration (McCain et al., 2023; Yokoyama et al., 2023).

The Sm-Nd isotope system is another valuable tool for sample and parent body characterization as it can provide chronological information and can help distinguish between different meteorite groups. Furthermore, the sensitivity of ^{149}Sm to thermal neutron capture can be used to deduce the history and conditions of cosmic ray exposure (CRE). Carbonaceous chondrites exhibit an approximately 30 ppm deficit in ^{142}Nd/^{144}Nd ratios compared to terrestrial rocks and are isotopically distinct from enstatite and ordinary chondrites where the ^{142}Nd/^{144}Nd deficit compared to terrestrial Nd is mostly in the range of 10–20 ppm (Andreasen & Sharma, 2006; Bouvier & Boyet, 2016; Boyet & Carlson, 2005; Boyet et al., 2018; Burkhardt et al., 2016; Carlson et al., 2007; Frossard et al., 2022; Fukai & Yokoyama, 2017; Gannoun et al., 2011; Johnston et al., 2022; Saji et al., 2020). As this deficit in ^{142}Nd/^{144}Nd is accompanied by elevated ^{145}Nd/^{144}Nd, ^{148}Nd/^{144}Nd, and ^{150}Nd/^{144}Nd ratios, the isotopic variations are best interpreted as nucleosynthetic in origin, reflecting a deficit in s-process Nd isotopes in carbonaceous chondrites compared to terrestrial Nd (Burkhardt et al., 2016; Carlson et al., 2007; Fukai & Yokoyama, 2017; Gannoun et al., 2011; Qin et al., 2011; Saji et al., 2020) along with some additional contribution to ^{142}Nd from the radioactive decay of short-lived ^{146}Sm in an Earth reservoir with superchondritic Sm-Nd ratio (Boyet & Carlson, 2005; Frossard et al., 2022; Johnston et al., 2022). Nucleosynthetic anomalies in Sm in carbonaceous chondrites are expressed primarily as an approximately 50–100 ppm deficit in ^{144}Sm/^{152}Sm ratios that is also distinct from those of enstatite and ordinary chondrites (Andreasen & Sharma, 2006; Carlson et al., 2007; Frossard et al., 2022). Apart from the ^{144}Sm anomaly, the main isotopic variability in Sm in extraterrestrial objects is caused by thermal and epithermal neutron capture on ^{149}Sm to create ^{150}Sm caused by exposure to galactic cosmic rays (e.g., Russ et al., 1971). Neutron capture products in meteorites can be used to characterize the irradiation and exposure history of meteorite parent bodies. In this work, we measured the Nd and Sm isotopic compositions of six carbonaceous chondrites and four samples of Ryugu to further evaluate potential genetic relationships between Ryugu samples and known chondrite groups, and to track the CRE history of Ryugu.

SAMPLES

The geological reference materials BCR-2 and BHVO-2 and the Smithsonian Allende Reference Powder were first processed and measured to verify the performance of the separation and purification chemistry methods and the accuracy and precision of the mass spectrometry analyses. Six carbonaceous chondrites, Allende (CV3), Murchison (CM2), Orgueil (CI1), Alais (CI1), Tarda (C2-ung), and Tagish Lake (C2-ung), were then analyzed followed by four Ryugu samples, A0106 and A0106–A0107 from the first touchdown and C0107 and C0108 from the second touchdown (Table 1).

METHODS

Sample Preparation and Column Chemistry

With the exception of the Allende powder dissolved at the Carnegie Institution for Science Earth and Planets Laboratory (EPL), all meteorite and Ryugu samples were first processed at Tokyo Institute of Technology following procedures described in Yokoyama et al. (2023). The

TABLE 1. Samples measured in this study, including the amount of Nd and Sm analyzed and the $^{147}Sm/^{144}Nd$ ratios for each sample calculated from the Sm and Nd concentration data reported by Yokoyama et al. (2023) and inferred from the measured $^{143}Nd/^{144}Nd$ of each sample.

Sample	Type	Nd (ng)	Sm (ng)	$^{147}Sm/^{144}Nd$[a]	$^{147}Sm/^{144}Nd$[b]
Geological reference materials					
BCR-2	Terrestrial	50[c]	13[c]		
BHVO-2	Terrestrial	50[c]	12[c]	0.248	
Meteorite samples					
Allende[d]	CV3	12.0	3.8	0.193	0.1925
Allende[e]	CV3	18.0	5.9	0.188	0.1924
Alais	CI1	7.2	2.3	0.193	0.1904
Orgueil	CI1	8.7	2.9	0.203	0.2018
Murchison	CM2	11.0	3.5	0.196	0.1946
Tarda	C2-ung	11.0	3.6	0.193	0.1944
Tagish Lake	C2-ung	10.0	3.3	0.194	0.1919
Ryugu samples					
A0106	Ryugu	7.7	2.5	0.198	0.1955
A0106-A0107	Ryugu	11.0	3.4	0.194	0.1958
C0107	Ryugu	6.9	2.2	0.193	0.1908
C0108	Ryugu	9.2	3.0	0.196	0.1948

[a]Values for $^{147}Sm/^{144}Nd$ calculated from Sm and Nd ID concentration measurements.
[b]Values for $^{147}Sm/^{144}Nd$ calculated based on the measured $^{143}Nd/^{144}Nd$, a chondritic initial $^{143}Nd/^{144}Nd$ (Bouvier et al., 2008) adjusted for the difference in $^{143}Nd/^{144}Nd$ measured for the standards in that study, and a closed Sm-Nd system since 4.568 Ga.
[c]For BCR-2 and BHVO-2, multiple sample aliquots of 50 ng each of Nd and 12–13 ng of Sm were processed and analyzed. The entirety of each meteorite and Ryugu sample aliquot was processed and measured as a single analysis.
[d]Smithsonian Allende powder dissolved at EPL. Sm and Nd concentration data from Boyet and Carlson (2005).
[e]Smithsonian Allende powder dissolved at Tokyo Institute of Technology.

sample dissolution procedures conducted at Tokyo Institute of Technology included ultrasonication followed by heating on a hot plate in a mixture of concentrated HF and HNO_3 in closed vials for 3–4 days. Samples were dried and then placed in a mixture of concentrated HNO_3 and HCl and heated on a hot plate in closed vials for 12 h. Samples were then treated with a mixture of HNO_3 and H_2O_2 to decompose organic matter. A small aliquot (~1%) of the dissolved sample solution was saved for determination of the $^{147}Sm/^{144}Nd$ ratio of each sample (see the Determination of $^{147}Sm/^{144}Nd$ Ratios Section). We cannot exclude that chemically resistant solar or presolar grains, for example SiC, survived this procedure, which can potentially affect isotopic anomalies for elements that would be present in significant quantities in those grains.

The REE fractions of the Ryugu and meteorite samples from an initial chromatography procedure at Tokyo Institute of Technology were shipped dry to EPL, where they were redissolved in a drop of concentrated HNO_3, dried, and then redissolved in the loading acid in preparation for column chemistry. A three-column procedure was used to purify Nd and Sm for analysis. The first two columns were run in tandem to remove Ce and separate Nd. The third column was necessary to provide a sufficiently clean fraction of Sm free of isobaric interferences from neighboring rare earth elements.

Column procedures were calibrated and tested for element yield and isotope fidelity using two basaltic geological reference materials, BCR-2 and BHVO-2, as well as a powdered bulk sample of Smithsonian Allende Reference Powder. These reference materials were digested at EPL. For the geological reference materials, approximately 15 mg of sample powder was dissolved in capped 15 mL Savillex PFA vials in a 2:1 mixture of concentrated HF:HNO_3 on a hot plate at 120°C for 48 h. The samples were then evaporated to dryness and treated twice with concentrated HNO_3 to eliminate fluorides. When dry from the second HNO_3 treatment, the samples were treated with a few drops of concentrated HCl and dried down. The samples were then dissolved in 2 mL of 6 M HCl and allowed to sit on the hot plate capped overnight. For the Allende reference material, approximately 50 mg of sample powder was digested in a 3 mL Savillex PFA beaker within a Parr bomb in a 2:1 mixture of concentrated HF:HNO_3 at 190°C for 7 days followed by treatment with concentrated HNO_3, evaporation to dryness, and treatment with 6 M HCl to eliminate fluorides.

Aliquots consisting of ~6 mg of material were then dried down and redissolved in the acids used for loading onto the first column. For the samples dissolved at EPL, the REE were first separated as a group using 2 mL of

AG50W-X8 cation exchange resin in a Bio-Rad 0.8 cm diameter by 3.8 cm long Poly-Prep column. After digestion, the sample was dissolved and loaded onto the column in 2.5 M HCl after which the major elements were eluted in additional 2.5 M HCl and the REE eluted after switching to 6 M HCl. The equivalent of approximately 2 mg of material of the geological samples was loaded onto the next column for calibration. This amount of material was larger than the mass of the unknown samples but provided enough material to accurately calibrate and test the columns for sample sizes of ~50 ng of Nd and ~12 ng of Sm. Allende was then used to test a bulk composition and sample size (~12 ng of Nd, ~3.8 ng of Sm) that more closely resembled the Ryugu samples. The procedural blanks for sample dissolution and REE chemistry conducted at Tokyo Institute of Technology varied from 2.7 to 4.9 pg of Nd and 0.51 to 0.73 pg of Sm. At EPL, Nd blanks measured during the column development phase ranged from 16 to 45 pg. A single Sm blank measurement was 1 pg. These blank levels were negligible compared to the 7–18 ng of Nd and 2–6 ng of Sm per sample that were processed for isotopic analyses of the meteorite and Ryugu samples.

Nd Separation

Nd was separated using a modified version of the tandem-column procedure detailed in Wang and Carlson (2022). This method consisted of a Ce oxidation column and a DGA column run jointly with the Ce oxidation column positioned above the DGA column reservoir. These column procedures previously have been shown to limit isotopic variability in Nd induced by ion-exchange column effects (Wang & Carlson, 2022). Resin cleaning and conditioning steps were completed separately for each column before placing the columns in this configuration. For the Ce oxidation column, 0.5 mL of Ln resin (50–100 μm, Eichrom) was loaded in a Bio-Rad Mini Bio-Spin polypropylene column. A solution of 10 M HNO_3-20 nM $NaBrO_3$ was used to oxidize Ce^{3+} to Ce^{4+}; the oxidized Ce was absorbed onto the Ln resin, while trivalent REEs passed through the column. This allowed a Ce-free eluent to drip onto the DGA column below. The resin bed was cleaned with 5 mL of 6 M HCl, 2 mL of 18 MΩ H_2O, and 6 mL of 10 M HNO_3, followed by 2 mL of 10 M HNO_3-20 nM $NaBrO_3$ for conditioning.

For the DGA column, a Muromac polypropylene Mini-column S was filled with 1 mL of DGA-N resin (50–100 μm, Eichrom). A top frit was used to pack the column and prevent the DGA-N resin from floating in the high normality HNO_3. This top frit also inhibited resin disturbance as drops fell into the reservoir from the above column. The resin bed was cleaned with 30 mL of 0.05 M HCl and 5 mL of 18.2 MΩ H_2O, followed by 6 mL of 10 M HNO_3 for conditioning.

The samples were loaded in 0.5 mL of 10 M HNO_3-20 nM $NaBrO_3$, which was made fresh on the day the procedure was performed. LREEs were eluted with 3 mL of 10 M HNO_3-20 nM $NaBrO_3$, and this eluent dripped into the reservoir of the DGA column below. After this step, the Ce oxidation column was removed and Nd was purified using only the DGA column. Na, Ba, and any remaining matrix elements were eluted with 10 mL of 3 M HNO_3. La and Pr were eluted with 14 mL of 2.5 M HCl. Nd was eluted and collected with 15 mL of 2.5 M HCl, followed by 1 mL of 1 M HCl. Sm was then eluted and collected in 8 mL of 0.1 M HCl. The initial DGA column did not produce a sufficiently clean Sm fraction, so the Sm fraction was processed on an additional column. The Nd fractions were dried down and treated with concentrated HNO_3 in preparation for filament loading. The Sm fractions were dried, treated with concentrated HNO_3 to remove any organics from the DGA resin, dried again, and dissolved in 0.1 mL of 0.45 N HCl in preparation for the final column.

Sm Separation

The final column used Ln resin (20–50 μm, Eichrom) to separate the Sm from any remaining Nd and HREEs. The column was 8 cm in height and 4 mm in diameter, which equated to approximately 400 mg of dry resin. The resin bed was cleaned with ~20 mL of 0.5 M HCl, followed by ~20 mL of 6 M HCl; the resin was subsequently conditioned with 3.5 mL of 0.45 M HCl. The samples were loaded in 0.1 mL of 0.45 M HCl. After two 0.1 mL rinses with 0.45 M HCl, any remaining Nd was eluted with 2.5 mL of 0.45 M HCl. Sm was then eluted and collected in 3.5 mL of 0.45 M HCl. The Sm fractions were dried and treated with concentrated HNO_3 prior to filament loading. Additional tests were run using the AMES Sm, BHVO-2, and Allende standards to ensure that the column procedure did not induce isotopic fractionation of Sm (Table S1).

Mass Spectrometry (TIMS)

Filament Loading

After column separation and treatment with HNO_3, the Nd and Sm fractions were redissolved in a microliter or two of 3 M HCl and loaded onto pre-degassed zone-refined Re filaments in a double filament assembly. The samples were loaded in the middle third of the filament between melted Parafilm dams to prevent samples from spreading across the filament. Filaments were held at 0.6 A during sample loading. Nd samples were loaded followed by 1 μL of 0.035 M H_3PO_4 solution. Once samples were dried at 0.6 A, the current was increased slowly until the filament glowed dull red for a second at approximately 2 A before being turned down. For both

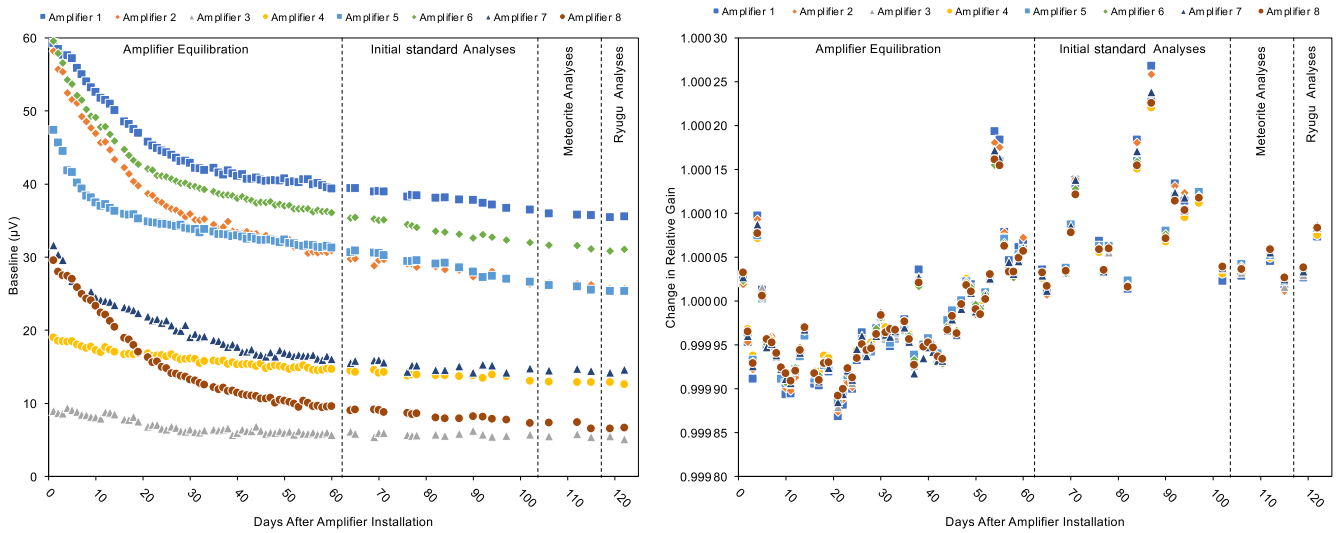

FIGURE 1. The electronic baseline (left) and the change in relative gain (right) performed with 10^{13} Ω amplifiers using the 3.3 pA calibration board from the time of amplifier installation through the time of Ryugu sample analyses. The change in relative gain is calculated by dividing the individual amplifier relative gains returned from the gain calibration procedure by the average of all the relative gains reported for that amplifier during the time window of these measurements. Dashed lines separate the periods of amplifier equilibration, initial standard analyses, meteorite analyses, and Ryugu sample analyses. Standards were also measured throughout the meteorite and Ryugu sample analysis periods. The factory installed ninth amplifier used in this study, which was in the amplifier housing since delivery and installation in February 2019, had somewhat different baseline and gain values and is not shown in this figure. Its average baseline was −13 μV with a total drift of 6 μV over the time window shown in this figure, and its change in relative gain closely matched those of the other amplifiers. (Color figure can be viewed at wileyonlinelibrary.com)

Nd and Sm, the entire aliquot for each meteorite and Ryugu sample was loaded onto one filament due to the small sample sizes.

Mass Spectrometry Methods

The Nd and Sm isotopic compositions were measured statically using nine Faraday cups, all equipped with 10^{13} Ω amplifiers, on the EPL Triton XT thermal ionization mass spectrometer (TIMS). The newly installed 10^{13} Ω amplifiers were allowed to equilibrate for approximately 2 months before analyses began. Amplifier decay constants were then measured by jumping from peak tops of 1 pA to background with the amplifier time constant corrections adjusted so that the signal on all Faraday cups returned to within ±0.05% of background within 10 s. Calibration of the amplifier gains used a 3.3 pA calibration source followed by 20 min of baseline at the end of the gain calibration procedure (Figure 1). In order to minimize the consequences of the long decay times of the high-gain amplifiers, these gain and background values were used for all sample and standard measurements that day so that once the static signal analyses began, the ion beams were not moved from their respective Faraday cups until the analysis was complete. The meteorite and Ryugu samples were measured in four different sample batches: meteorite Nd analyses, meteorite Sm analyses, Ryugu Nd analyses, and Ryugu Sm analyses. Each sample batch was run in its entirety on a single day of measurements, and standards were measured alongside samples during each analytical run.

For Nd, samples and standards were run with the $^{142}Nd^{+}$ signal below the 5 pA limit of the amplifiers with a target of 270 ratios taken with 8 s signal integrations. Not all samples ran for this duration. Table S1 includes the average signal size and number of ratios measured for each sample. Neodymium isotopic compositions are corrected for mass fractionation to $^{146}Nd/^{144}Nd = 0.7219$ assuming the exponential law. No residual correlations were seen between any fractionation corrected Nd isotope ratio with the raw measured $^{146}Nd/^{144}Nd$ ratio indicating that the runs were following the expected exponential mass fractionation. Several standards (JNdi-1) were included within each sample barrel. Over the eight barrels involved in the sample analyses, 17 analyses of JNdi-1 were measured (Table S1). These analyses showed 2 SE uncertainties of 15, 13, 10, 16, and 21 ppm for $^{142}Nd/^{144}Nd$, $^{143}Nd/^{144}Nd$, $^{145}Nd/^{144}Nd$, $^{148}Nd/^{144}Nd$, and $^{150}Nd/^{144}Nd$, respectively. Potential interferences from Ce and Sm were monitored at m/z = 140 and 147, respectively. The measured $^{140}Ce/^{146}Nd$ and $^{147}Sm/^{146}Nd$ ratios for each sample are reported in Table S1.

Sm analyses involved signal sizes of $^{149}Sm^{+}$ targeted at 1 pA and 270 ratios taken at 8 s of signal integration. None of the meteoritic or Ryugu samples produced signals of this duration; the average signal size and number of ratios for each sample are included in Table S1. Samarium isotopic

compositions are corrected for mass fractionation using the exponential law to $^{147}Sm/^{152}Sm = 0.56081$. Potential interferences were monitored at $m/z = 146$ (Nd) and either 155 or 156. The $m/z = 155$ signal can include $^{155}Gd^+$, $^{139}La^{16}O^+$, and $^{136}Ba^{19}F^+$, and all of these have other isotopic species that interfere with Sm, most prominently $^{154}Sm^+$. Whereas LaO^+ only interferes at $m/z = 154$, Gd^+ also presents a small interference on $^{152}Sm^+$ ($^{152}Gd/^{155}Gd \sim 0.09$), and BaF^+ presents a relatively small interference on $^{148}Sm^+$ ($^{130}Ba/^{136}Ba \sim 0.014$). CeO^+ is another potential interference for $^{152}Sm^+$ and $^{154}Sm^+$ but can be monitored only at $m/z = 156$ and 158. Besides $^{140}Ce^{16}O^+$, $m/z = 156$ also potentially includes $^{156}Gd^+$ and $^{137}Ba^{19}F^+$, but only minor isotopologues of LaO^+ ($^{138}La^{18}O^+$ and $^{139}La^{17}O^+$). All early analyses monitored mass 155, but concern over the possible contribution of CeO^+ and lack of evidence for LaO^+ led us to shift the interference monitor to $m/z = 156$ before the analyses of Orgueil and all the Ryugu samples, as well as the last few runs of AMES and BHVO (Table S1). In TIMS analysis, the signal sizes of Sm and the various potential interfering species varied independently during the course of each analysis such that the ratio of the $m/z = 155$, 156 signal, if present, to $m/z = 152$ signal would change throughout the run. When the interferences were significant, before correcting for the interference measured at $m/z = 155$ or 156, some samples displayed a strong correlation between the 154/152 and 155/152 or 156/152 ratios during the analysis. Because the ratios 154/155 or 154/156 for the potential interfering species are considerably different, the choice of interfering species was determined by selecting which correction removed the correlation between 154/152 and 155,156/152 ratios. For example, for the interferences detected at $m/z = 155$, the proportional contributions to the $m/z = 154$ signal relative to the $m/z = 155$ signal are 0.0009 for $^{138}La^{16}O^+/^{139}La^{16}O^+$, 0.147 for $^{154}Gd^+/^{155}Gd^+$, and 0.839 for $^{135}Ba^{19}F^+/^{136}Ba^{19}F^+$. For interferences detected at $m/z = 156$, these ratios are 0.106 for $^{154}Gd^+/^{156}Gd^+$, 0.0028 for $^{138}Ce^{16}O^+/^{140}Ce^{16}O^+$, and 0.588 for $^{135}Ba^{19}F^+/^{137}Ba^{19}F^+$. A good example of how this correction was done is the analysis of Murchison where the 155/152 ratio was near zero for the first 40 ratios but gradually rose to a peak of 0.012 at ratio 120 after which it declined rapidly. Before applying an interference correction, the fractionation corrected 154/152 ratio rose from 0.850 at the beginning of the run to 0.861 at ratio 120. No other Sm isotope ratio showed a resolved correlation with 155/152. Assuming that mass 155 was either $^{139}La^{16}O^+$ or $^{155}Gd^+$, and applying a correction to mass 154 on that basis, did not remove the 155/152–154/152 correlation. In contrast, assuming $m/z = 155$ was $^{136}Ba^{19}F^+$ and applying an appropriate correction based on standard Ba isotopic composition, the 155/152–154/152 correlation was eliminated resulting in corrected average $^{154}Sm/^{152}Sm$ of 0.8510 ± 0.0005 (2σ) for the first 10 ratios and 0.8510 ± 0.0008 for the average of the 10 ratios centered around ratio 120.

We tested this interference correction procedure by running AMES Sm doped with small amounts of Gd and Ba. In each case, the correct interfering species was identified through the 154/152 versus 155,156/152 correlation resulting in interference corrected isotopic compositions that overlapped within uncertainty with those measured for the AMES standard (see Table S1). In all cases where a correlation was seen between 154/152 and 155,156/152, except for Alais and two of the BHVO-2 analyses, the correlation was removed by assuming that the interfering species was solely BaF^+. For Alais and two of the BHVO-2 analyses, no solution could be found that effectively removed the observed correlation between 154/152 and 155/152 suggesting that CeO^+ might have been present during these analyses along with BaF^+, leading us to switch the interference monitor to mass 156. As a result, the uncertainties on the $^{154}Sm/^{152}Sm$ ratios for these analyses are considerably higher than in the other analyses. In addition, the reproducibility of $^{149}Sm/^{152}Sm$ and $^{150}Sm/^{152}Sm$ for the five analyses of BHVO-2 is at least five and eight times, respectively, higher than the reproducibility achieved on three analyses of BCR-2, and the 16 analyses of the AMES Sm standard, suggesting that an uncorrected interference from CeO^+ on $^{152}Sm^+$ may have been propagated into these ratios as a result of the fractionation correction.

All the data measured in this study are reported in Table S1 with the reduced data for the meteoritic and Ryugu samples reported in Table 2 of the text. The ratios in Table 2 are expressed as the part per million (μ) deviations from the average value of all the standards measured during the sample analyses. $\mu^iNd = [(^iNd/^{144}Nd)_{sample}/(^iNd/^{144}Nd)_{standard} - 1] \times 10^6$ and $\mu^iSm = [(^iSm/^{152}Sm)_{sample}/(^iSm/^{152}Sm)_{standard} - 1] \times 10^6$. The $\mu^{142}Nd_c$ data in Table 2 are the $\mu^{142}Nd$ values that have been corrected for radiogenic ^{142}Nd variations resulting from ^{146}Sm decay to a value corresponding to the average chondritic value of $^{147}Sm/^{144}Nd = 0.1960$ (Bouvier et al., 2008) and are simply referred to as $\mu^{142}Nd$ or $^{142}Nd/^{144}Nd$ ppm throughout the remainder of the text.

Determination of $^{147}Sm/^{144}Nd$ Ratios

The $^{147}Sm/^{144}Nd$ ratio of each sample except the Allende powder dissolved at EPL was determined at Tokyo Institute of Technology by the isotope dilution (ID) technique (Kagami & Yokoyama, 2016). In brief, a mixed spike enriched in ^{145}Nd (91.73%) and ^{149}Sm (97.68%) was added to a small aliquot (~1%) of the decomposed sample solution that was conditioned in 0.5 M HNO_3. The $^{145}Nd/^{146}Nd$ and $^{149}Sm/^{147}Sm$ ratios

TABLE 2. Nd and Sm isotopic compositions of the reference materials, meteorites, and Ryugu samples measured in this study. The $\mu^{143}Nd$ data are calculated relative to the average chondrite $^{143}Nd/^{144}Nd$ (Bouvier et al., 2008) adjusted for the difference in $^{143}Nd/^{144}Nd$ measured for the laboratory standard in that study and that measured here. The full isotopic results are presented in Table S1.

Sample	$\mu^{142}Nd_m$[a]	$\mu^{142}Nd_c$[b]	$\mu^{143}Nd$	$\mu^{145}Nd$	$\mu^{148}Nd$	$\mu^{150}Nd$	$\mu^{144}Sm$	$\mu^{148}Sm$	$\mu^{149}Sm$	$\mu^{150}Sm$	$\mu^{154}Sm$
Terrestrial standards											
BCR-2[c]	−3 ± 21		−50 ± 21	22 ± 9	19 ± 21	70 ± 32	−58 ± 230	3 ± 2	−36 ± 23	−29 ± 17	−13 ± 52
BHVO-2[d]	−3 ± 11		632 ± 8	34 ± 18	19 ± 22	47 ± 52	−106 ± 139	−1 ± 23	55 ± 126	41 ± 132	52 ± 49
Meteorite samples											
Allende[e]	−53 ± 21	−48 ± 21	−208 ± 17	33 ± 16	0 ± 27	38 ± 40	120 ± 65	−26 ± 16	−30 ± 54	82 ± 267	−90 ± 104
Allende[f]	−38 ± 34	−33 ± 34	−214 ± 27	54 ± 26	37 ± 41	9 ± 55	−50 ± 83	−71 ± 38	−44 ± 33	79 ± 49	−117 ± 49
Alais	−51 ± 87	−43 ± 89	−333 ± 73	44 ± 82	−42 ± 117	−53 ± 157	136 ± 139	−103 ± 57	−169 ± 54	532 ± 65	15 ± 264
Orgueil	−65 ± 37	−73 ± 38	340 ± 29	17 ± 26	40 ± 54	199 ± 72	168 ± 140	−73 ± 52	−235 ± 47	333 ± 66	−215 ± 97
Murchison	−27 ± 40	−25 ± 41	−81 ± 34	88 ± 32	−26 ± 45	13 ± 67	−51 ± 77	−42 ± 37	−5 ± 32	−16 ± 43	−46 ± 45
Tarda	−27 ± 32	−24 ± 32	−93 ± 26	41 ± 22	40 ± 43	69 ± 61	14 ± 77	−72 ± 33	−41 ± 35	214 ± 42	−223 ± 60
Tagish Lake	−82 ± 41	−76 ± 42	−241 ± 32	2 ± 28	−29 ± 53	3 ± 69	−23 ± 217	16 ± 98	−14 ± 73	37 ± 69	−85 ± 109
Ryugu samples											
A0106	−110 ± 44	−109 ± 45	−28 ± 37	10 ± 35	27 ± 64	70 ± 81	−65 ± 83	−97 ± 42	−138 ± 33	276 ± 49	51 ± 49
A0106-A0107	−91 ± 65	−90 ± 66	−14 ± 56	48 ± 57	−39 ± 74	42 ± 105	−5 ± 71	−73 ± 37	−83 ± 27	111 ± 39	−3 ± 47
C0107	−103 ± 37	−95 ± 38	−308 ± 31	25 ± 32	42 ± 49	126 ± 70	−47 ± 53	26 ± 22	−67 ± 23	49 ± 26	36 ± 26
C0108	−22 ± 38	−20 ± 39	−69 ± 33	−28 ± 29	−20 ± 51	63 ± 62	190 ± 241	−67 ± 96	−9 ± 96	236 ± 111	−72 ± 108

[a]Measured $\mu^{142}Nd$ values.

[b]$\mu^{142}Nd$ values corrected for radiogenic ^{142}Nd variations resulting from ^{146}Sm decay based on the Sm-Nd ratios calculated from measured $^{143}Nd/^{144}Nd$ to a value corresponding to the average chondritic value of $^{147}Sm/^{144}Nd = 0.1960$ (Bouvier et al., 2008) and referred to as simply $\mu^{142}Nd$ throughout the remainder of the text. The analytical uncertainties of the corrected values differ slightly from those of the uncorrected values due to the propagation of the uncertainties during the correction calculation.

[c]For BCR-2, $n = 3$ for Sm and $n = 4$ for Nd.

[d]For BHVO-2, $n = 5$ for Sm and $n = 4$ for Nd.

[e]Smithsonian Allende Reference Powder dissolved at EPL.

[f]Smithsonian Allende Reference Powder dissolved at Tokyo Institute of Technology.

in the spiked samples were then measured by inductively coupled plasma mass spectrometry (ICP-MS: iCAP TQ, Thermo Fisher Scientific) without chemical separation. Data were acquired in the SQ non-gas mode with 10 ms integration/mass, 100 sweeps/run, and 30 runs/measurement. Instrumental mass bias was corrected by repeated measurements of a mixed REE standard solution (XSTC-1, SPEX). The typical analytical uncertainty of the $^{147}Sm/^{144}Nd$ ratio was ~1% (2SE). The accuracy of the procedure was confirmed by measuring the Sm-Nd ratio of a reference rock sample (BHVO-2), which agreed with literature data (Jochum et al., 2016) within ±1%.

RESULTS

The average values measured for JNdi-1 using the techniques described here differ somewhat from higher precision data measured dynamically on much larger signals using 10^{11} Ω amplifiers (e.g., Garçon et al., 2018), showing $^{142,143}Nd/^{144}Nd$ ratios elevated by 75–80 ppm and $^{145,148,150}Nd/^{144}Nd$ ratios lower by 45–58 ppm, although the average value measured here overlaps within 2 SDs of the higher precision data. Analyses of the geological standards BCR-2 and BHVO-2 show Nd isotopic compositions similar to the average obtained for JNdi-1 where the 2-sigma mean uncertainty for multiple measurements of these standards were 11–21 ppm for $^{142}Nd/^{144}Nd$, and 32–52 ppm for $^{150}Nd/^{144}Nd$ for BHVO-2 and BCR-2, respectively. Both geological standards returned slightly high (22–34 ppm) averages for $^{145}Nd/^{144}Nd$, but the average of $^{142}Nd/^{144}Nd$ for both standards differed from the JNdi-1 average by only −3 ppm. Samarium data for the geological standards overlap within uncertainty with the averages obtained for the AMES Sm standard although the reproducibility for BHVO-2 is considerably poorer than for BCR-2 as a result of the interference correction issues mentioned previously.

All meteorites analyzed here show deficits in $^{142}Nd/^{144}Nd$ compared to terrestrial Nd, although four of the seven analyses overlap the terrestrial standard value within uncertainty (Figure 2 and Table 2). Our data agree with previous measurements that found no clear ^{142}Nd isotopic heterogeneity among carbonaceous chondrites for $\mu^{142}Nd$, although Fukai and Yokoyama (2017) showed that even within errors, $\mu^{142}Nd$ in bulk carbonaceous chondrites correlates with $\mu^{148}Nd$ and $\mu^{150}Nd$ following an s-process mixing line, hinting at the presence of barely resolvable nucleosynthetic anomalies. The weighted mean of the meteorite data measured here shows only $^{142}Nd/^{144}Nd$ (−48 ± 15 ppm, 2 sigma mean) and $^{145}Nd/^{144}Nd$ (37 ± 21 ppm) to be resolved from the terrestrial standard. For unclear reasons, the Nd analysis

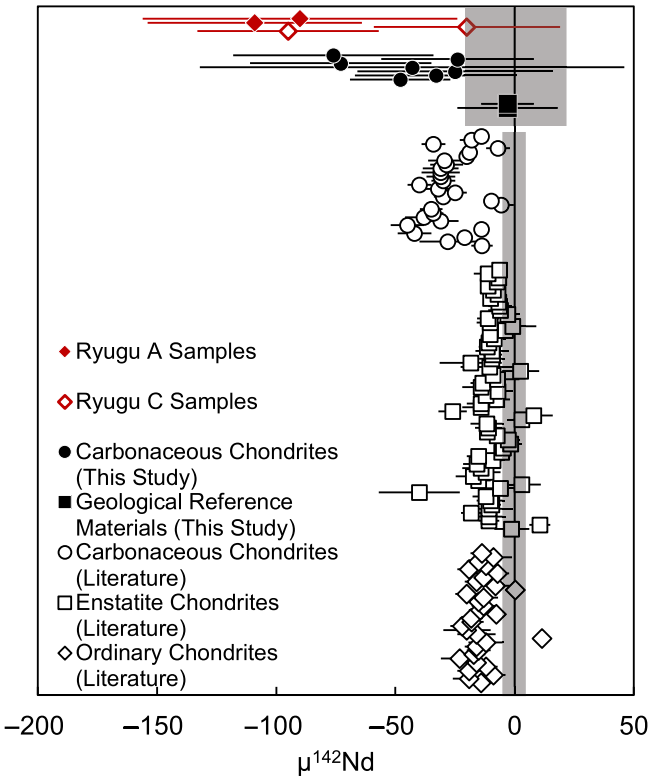

FIGURE 2. The $\mu^{142}Nd$ compositions of Ryugu "A" (solid red diamonds) and "C" (open red diamonds) samples, carbonaceous chondrites (black circles), and geological reference materials (black squares) from this study and ordinary chondrites (white diamonds), enstatite chondrites (white squares), and carbonaceous chondrites (white circles) from previous studies (Andreasen & Sharma, 2006; Boyet et al., 2018; Bouvier & Boyet, 2016; Boyet & Carlson, 2005; Burkhardt et al., 2016; Carlson et al., 2007; Frossard et al., 2022; Fukai & Yokoyama, 2017, 2019; Gannoun et al., 2011; Johnston et al., 2022; Saji et al., 2020). The data from this study and most previous studies are corrected for ^{146}Sm decay to an average chondritic $^{147}Sm/^{144}Nd = 0.1960$ (Bouvier et al., 2008). The gray shaded regions indicate the 2SD of our repeated measurements of the BCR-2 standard (±21 ppm) and the average 2SD of previous measurements (±5 ppm). (Color figure can be viewed at wileyonlinelibrary.com)

of Alais was plagued by a small signal, short duration run, and significant interference from Ce resulting in increased measurement uncertainties. No other meteorite sample was compromised to this extent. The Ryugu samples similarly all show deficits in $^{142}Nd/^{144}Nd$, with only one sample (C0108) not resolved from the terrestrial standard. The weighted mean of the Ryugu samples shows significantly low $\mu^{142}Nd$ (−75 ± 40) and elevated $\mu^{150}Nd$ (80 ± 36) relative to the terrestrial standard.

For the Sm data, none of the meteorites or Ryugu samples show $^{144}Sm/^{152}Sm$ resolved convincingly from the terrestrial standard given their uncertainties. The most obvious isotopic contrast is in the ratios of $^{149,150}Sm/^{152}Sm$

for some samples that show deficits in ^{149}Sm and excesses in ^{150}Sm as expected for neutron capture on ^{149}Sm. This is most obvious in the two CI chondrites measured here (Alais, Orgueil, Table 2) and less so in the Ryugu samples where three of the four samples have resolved deficits in ^{149}Sm and all four have resolved excesses in ^{150}Sm. Calculating the weighted means for the "A" and "C" Ryugu samples separately suggests that the "A" samples may have larger effects (μ^{149}Sm = −110 ± 55, μ^{150}Sm = 193 ± 165) than the "C" samples (μ^{149}Sm = −38 ± 58, μ^{150}Sm = 142 ± 187), though the data overlap within uncertainty (Table S1).

DISCUSSION

Nd Isotopic Compositions

Ordinary, enstatite, and carbonaceous chondrites exhibit deficits in ^{142}Nd/^{144}Nd compared to modern terrestrial rocks (Andreasen & Sharma, 2006; Bouvier & Boyet, 2016; Boyet & Carlson, 2005; Boyet et al., 2018; Burkhardt et al., 2016; Carlson et al., 2007; Frossard et al., 2022; Fukai & Yokoyama, 2017; Gannoun et al., 2011; Johnston et al., 2022; Saji et al., 2020). This deficit is accompanied by elevated ^{145}Nd/^{144}Nd, ^{148}Nd/^{144}Nd, and ^{150}Nd/^{144}Nd ratios, indicating that the negative μ^{142}Nd of the chondrites are best interpreted as nucleosynthetic in origin, reflecting a deficit in s-process Nd isotopes in all chondrites, and especially carbonaceous chondrites, compared to terrestrial Nd. Carbonaceous chondrites measured in previous studies exhibit an average μ^{142}Nd deficit of ∼30 ppm. The carbonaceous chondrites measured here range to more negative values but overlap with previous higher precision measurements within the larger analytical uncertainties associated with the low amounts of Nd measured here (Figure 2 and Table 2). The data for Orgueil and Tagish Lake measured here (μ^{142}Nd = −73 ± 38, −76 ± 42, respectively) compare to −28 ± 12 reported by Carlson et al. (2007) for Orgueil and −18 ± 5 for Tagish Lake reported by Fukai and Yokoyama (2017), reflecting the tendency of the data measured here toward larger apparent deficits in ^{142}Nd than reported previously for the same meteorites. The cause of this is unclear. Possible causes include the high ^{142}Nd/^{144}Nd measured here for the JNdi-1 standard (Table S1), although the μ^{142}Nd values measured here for BCR-2 and BHVO-2 are offset from the JNdi-1 value by only 3 ppm, or that the dissolution of the meteorites did not completely dissolve s-process-rich presolar Si-carbide.

Three of the Ryugu samples exhibit μ^{142}Nd deficits that are resolved from zero while one value is negative but overlaps with zero within analytical uncertainty. All four Ryugu samples overlap within analytical uncertainties with carbonaceous chondrite compositions (Figure 2 and Table 2), but show a similar tendency toward lower ^{142}Nd/^{144}Nd as do the meteorite data. The weighted mean of all four Ryugu analyses shows μ^{142}Nd = −75 ± 40, again suggesting a larger ^{142}Nd deficit in Ryugu compared to carbonaceous chondrites, though the difference is not resolved within analytical uncertainties. The tendency of several of the meteorite analyses measured here toward lower μ^{142}Nd than higher precision data reported previously for larger sample measurements of the same meteorites cautions against overinterpretation of the significance of the more negative μ^{142}Nd in the Ryugu samples.

The larger analytical uncertainties associated with measuring small amounts of Nd preclude a higher resolution comparison between Ryugu samples and specific carbonaceous chondrite groups (i.e., CI chondrites), but nevertheless these results indicate a genetic relationship between Ryugu samples and carbonaceous chondrites, which is consistent with other isotope systems such as Ti and Cr (Yokoyama et al., 2023), Fe (Hopp et al., 2022), Cu and Zn (Paquet et al., 2022), Ca (Moynier et al., 2022), and O (Kawasaki et al., 2022; Yokoyama et al., 2023). Although the data for Allende and Murchison show small resolved excesses in ^{145}Nd/^{144}Nd, the ^{145}Nd/^{144}Nd and ^{148}Nd/^{144}Nd ratios measured for all Ryugu samples are not resolved from the terrestrial standard, but the four Ryugu samples average to a weighted mean of μ^{150}Nd = 80 ± 36, compared to a weighted mean of μ^{150}Nd of 45 ± 60 for the carbonaceous chondrites measured here. These compare with higher precision carbonaceous chondrite data measured on larger amounts of Nd that have μ^{150}Nd ranging from 0 to 60, with an average of 26 ± 7 reported by Fukai and Yokoyama (2017). Although the uncertainties are large, the μ^{145}Nd and μ^{150}Nd data for Ryugu and the carbonaceous chondrites measured here scatter along the r-, s-process mixing line defined by higher precision measurements of leaches of Orgueil (Frossard et al., 2022; Figure 3). These results provide further evidence of a genetic relationship between Ryugu and carbonaceous chondrites and may suggest a slightly larger s-process deficit in Ryugu compared to carbonaceous chondrites, although the uncertainties of the Ryugu data do not resolve that difference.

^{147,146}Sm–^{143,142}Nd Systematics

The isotope ^{147}Sm decays to ^{143}Nd with a half-life of 106 billion years, and the now extinct ^{146}Sm decays to ^{142}Nd with a half-life of 103 million years. Both have been used extensively as chronometers for early Solar System materials (e.g., Lugmair & Marti, 1977; Sanborn et al., 2015). On a ^{147}Sm–^{143}Nd isochron diagram, ordinary chondrites, enstatite chondrites, and carbonaceous chondrites scatter along a 4.568 Ga isochron (dashed black

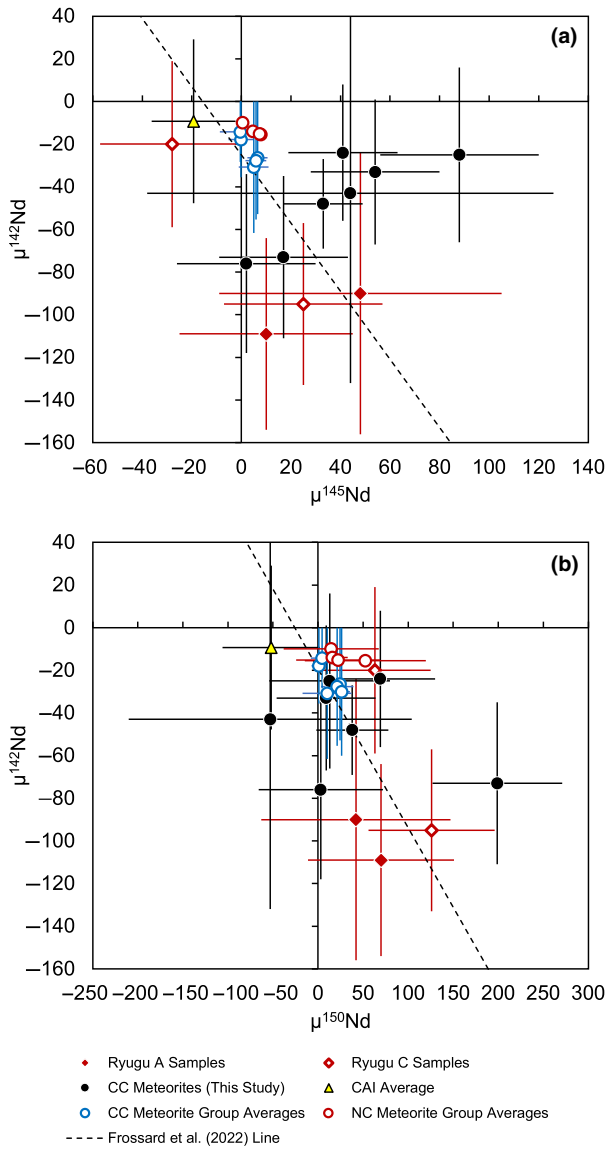

FIGURE 3. (a) μ^{142}Nd versus μ^{145}Nd and (b) μ^{142}Nd versus μ^{150}Nd for Ryugu "A" (solid red diamonds) and "C" (open red diamonds) samples and carbonaceous chondrites (black circles) from this study and CC (open blue circles) and NC (open red circles) meteorite group averages (Burkhardt et al., 2016; Frossard et al., 2022; Fukai & Yokoyama, 2017, 2019; Render & Brennecka, 2021; Saji et al., 2020) and the CAI average (yellow triangle; Brennecka et al., 2013; Bouvier & Boyet, 2016; Burkhardt et al., 2016; Shollenberger et al., 2018) from previous studies. The dashed r-, s-process mixing line represents high-precision measurements of leaches of Orgueil (Frossard et al., 2022). (Color figure can be viewed at wileyonlinelibrary.com)

line, Figure 4). Using the Sm-Nd ratios measured by isotope dilution ICP-MS (Determination of ^{147}Sm/^{144}Nd Ratios Section) the carbonaceous chondrites and Ryugu samples measured in this study also scatter along this line within their analytical uncertainties and within the range defined by chondrites (Figure 4). One chondrite sample (Allende) plots substantially to the left of the chondrite Sm-Nd correlation as a result of its low ^{147}Sm/^{144}Nd (0.188) compared to its ^{143}Nd/^{144}Nd that overlaps the high end of the range displayed by chondrites. While these results do not allow definition of a precise ^{147}Sm–^{143}Nd age for Ryugu, all four samples plot within the field of chondrite data that are consistent with a 4.568 Ga age. Given the limited spread in Sm-Nd and overlapping ^{142}Nd/^{144}Nd for the four Ryugu samples, no significant chronological information can be extracted from the ^{146}Sm–^{142}Nd data.

Sm Isotopic Compositions and CRE

Carbonaceous chondrites display depletions in the pure p-process ^{144}Sm of order 100 ppm compared to terrestrial Sm (Andreasen & Sharma, 2006; Carlson et al., 2007). Samarium-144 is a low abundance isotope (~3%). The external reproducibility on the ^{144}Sm/^{152}Sm ratios measured here is provided by the repeat analyses of the geological standards BHVO-2 and BCR-2 obtained on similar ion signal sizes as the samples. The 2 sigma mean uncertainties, in ppm, are 139 (BHVO-2; $n = 5$) and 230 (BCR-2; $n = 3$), respectively. Given these uncertainties, we cannot convincingly resolve a deficit in ^{144}Sm of ~100 ppm in any of the meteorite or Ryugu samples analyzed here.

Extraterrestrial materials have experienced irradiation with solar and galactic cosmic ray particles that can create isotopic variations in the near surface of airless bodies through spallation and neutron caption reactions with nuclei within the body (e.g., Eugster et al., 2006; Leya et al., 2000; Lingenfelter et al., 1961; Spergel et al., 1986). Samarium, together with Gd, have played key roles in cosmic ray irradiation studies of extraterrestrial rocks as dosimeters of secondary neutron capture. For Sm, the significant nuclear reaction is capture of thermal and epithermal neutrons by ^{149}Sm to create ^{150}Sm (e.g., Hidaka et al., 2017; Russ et al., 1971) resulting in lowered ^{149}Sm/^{152}Sm and correspondingly elevated ^{150}Sm/^{152}Sm. The largest previously measured deficit in ^{149}Sm in carbonaceous chondrites was observed in the CI chondrite Orgueil (μ^{149}Sm = −233 ± 13; Carlson et al., 2007). The CI chondrites measured in this study, Orgueil (μ^{149}Sm = −235 ± 47) and Alais (μ^{149}Sm = −169 ± 54) show larger ^{149}Sm deficits than the CV, CM, and ungrouped chondrites, with the largest ^{149}Sm deficit exhibited by Orgueil, which overlaps with the value from Carlson et al. (2007; Figure 5). The CV, CM, and ungrouped chondrites measured in this study exhibit μ^{149}Sm values that overlap with previous carbonaceous chondrite measurements and with zero within the analytical uncertainties (Figure 4 and Table 2).

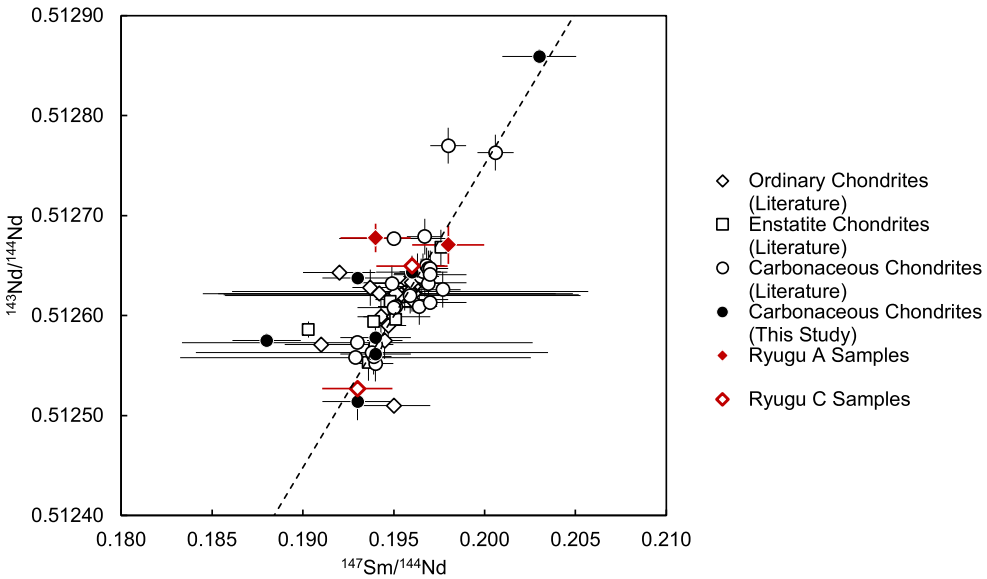

FIGURE 4. ^{147}Sm–^{143}Nd isochron diagram including data for Ryugu "A" (solid red diamonds) and "C" (open red diamonds) samples and carbonaceous chondrites (black circles) measured in this study and ordinary chondrites (white diamonds; Bouvier et al., 2008; Boyet & Carlson, 2005; Fukai & Yokoyama, 2017), enstatite chondrites (white squares; Bouvier & Boyet, 2016; Bouvier et al., 2008; Boyet & Carlson, 2005), and carbonaceous chondrites (white circles; Bouvier et al., 2008; Boyet & Carlson, 2005; Fukai & Yokoyama, 2017) from previous studies. The black dashed line is a 4.568 Ga chondrite isochron (Bouvier et al., 2008). (Color figure can be viewed at wileyonlinelibrary.com)

Three of the Ryugu samples (A0106, A0106-A0107, and C0107) exhibit negative $\mu^{149}Sm$ values that are resolvable from zero and within the range of carbonaceous chondrites, while the fourth (C0108) has a smaller $\mu^{149}Sm$ deficit that overlaps within uncertainty with zero as well as with the data for two of the other Ryugu samples. The data for C0108 have larger than normal uncertainties because of a run marked by small signal size, limited duration, and significant signal at the mass 156 interference monitor (Table S1). Although C0108 has a near-zero $\mu^{149}Sm$, its $\mu^{150}Sm$ shows the largest excess of the Ryugu samples, suggesting that its irradiation history is more akin to the other three Ryugu samples than is suggested by its relatively small deficit in ^{149}Sm.

Capture of neutrons by elements in meteorites that have high neutron capture cross sections can be used to characterize the irradiation and exposure history of meteorite parent bodies. In the case of Sm, the large thermal neutron cross section of ^{149}Sm facilitates the formation of the stable isotope ^{150}Sm. The measurement of $^{150}Sm/^{149}Sm$ therefore enables the estimation of the neutron fluence experienced by samples (e.g., Hidaka et al., 2000, 2009; Lingenfelter et al., 1972; Russ et al., 1971). The Sm isotopic composition of a sample in combination with its Gd isotopic composition can also potentially yield information regarding the composition and size of the parent body and the original depth of a meteorite sample on the parent body because neutron production rates and their energy distribution depend on depth and the target material composition. Because the peaks in neutron capture cross sections for ^{149}Sm (0.0973 eV) and ^{157}Gd (0.0314 eV) occur at different neutron energies, the magnitude of isotopic changes to Sm and Gd in samples that have experienced CRE can be used to estimate the energy spectrum of the neutrons, and hence the depth in the body where the neutron exposure occurred (e.g., Hidaka et al., 2017). Unfortunately, we were not able to obtain Gd isotopic data for the Ryugu samples, so we have no information on the neutron energy spectrum experienced by these samples and can only estimate the total integrated neutron flux experienced by the samples studied here. The $^{150}Sm/^{152}Sm$ and $^{149}Sm/^{152}Sm$ ratios for the carbonaceous chondrites and Ryugu samples measured in this study fall along a correlation line resulting from changing one atom of ^{149}Sm to ^{150}Sm (Figure 6), indicating that these isotopic variations are the result of thermal neutron capture on ^{149}Sm from the exposure to galactic cosmic rays. Neutron fluence can also modify the Nd isotopic composition of samples, but this effect is too small to alter the Nd isotopic compositions reported here beyond the analytical uncertainties.

To calculate the neutron fluence ψ (expressed as neutrons per cm^2) experienced by the samples studied here, we use the relationship between ψ and $\mu^{149}Sm$ expressed by the equation

$$\psi = \left(-1.0 \times 10^{-6} \times \mu^{149}Sm\right)/\sigma_{149},$$

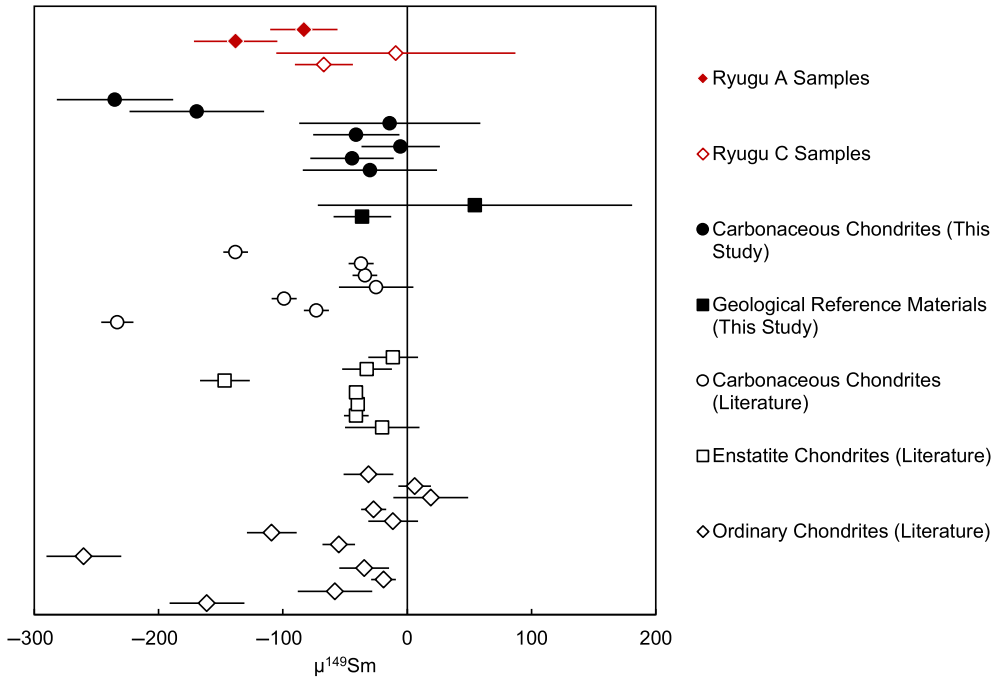

FIGURE 5. The μ^{149}Sm compositions of Ryugu "A" (solid red diamonds) and "C" (open red diamonds) samples, carbonaceous chondrites (black circles), and geological reference materials (black squares) from this study and carbonaceous chondrites (white circles; Boyet & Carlson, 2005; Carlson et al., 2007), enstatite chondrites (white squares; Bouvier & Boyet, 2016; Boyet & Carlson, 2005; Carlson et al., 2007; Frossard et al., 2022), and ordinary chondrites (white diamonds; Boyet & Carlson, 2005; Carlson et al., 2007; Frossard et al., 2022) from previous studies. (Color figure can be viewed at wileyonlinelibrary.com)

where μ^{149}Sm is the measured value for the sample and σ_{149} the thermal neutron capture cross section (σ_{th}) of ^{149}Sm. We assume a constant rate of cosmic ray irradiation and use $\sigma_{th} = 4.014 \times 10^{-20}$ cm^2 (Mughabghab, 1984), which is lower than the purely thermal neutron capture of 4.0511×10^{-20} cm^2 in order to approximate the effects of shielding depth and bulk composition on the neutron energy spectrum where the neutron capture occurred (e.g., Hidaka et al., 2000).

The calculated neutron fluence values for each sample studied here are shown in Table 3 and Figure 7. There is much overlap between the Ryugu samples within the uncertainties, but generally the "A" samples record a larger neutron fluence ("A" average = $(2.75 \pm 1.94) \times 10^{15}$ n cm^{-2}) than the "C" samples ("C" average = $(0.95 \pm 2.04) \times 10^{15}$ n cm^{-2}). Although both "A" and "C" samples were collected from the surface of Ryugu, the "C" samples were collected from near the area excavated by the cratering experiment and hence could contain material originally residing at depth within Ryugu. Data from ^{10}Be abundances in the Ryugu samples have been used to estimate that the "C" samples record a depth of 50–120 g cm^{-2} while the "A" samples record a depth of <5–15 g cm^{-2} (Nishiizumi et al., 2022). This corresponds to an origin just below the surface for the "A" samples and a depth of 0.7–1.3 m for the "C" samples, which approaches the 1.7 m depth of the artificial crater (Arakawa et al., 2020; Nishiizumi et al., 2022; Okazaki et al., 2022), although this may not be directly comparable to the depth of origin of the samples measured here for their Sm isotopic compositions because the "A" and "C" samples measured in this study are different aliquots than the "A" and "C" samples measured in previous studies. Additionally, the differences resolved by ^{10}Be may not be applicable to the Sm data since the Sm neutron capture integrates exposure over longer time intervals than does ^{10}Be.

Multiple studies have aimed to constrain the CRE age of Ryugu. Cratering statistics indicate that materials shallower than 1 m were mixed vertically over time scales of 1000–100,000 years (Takaki et al., 2022), much faster than would be resolved by the Sm data. Analyses of ^{10}Be abundances of Ryugu samples yielded a minimum ^{10}Be exposure age of 4.1 Myr (Nishiizumi et al., 2022). Analyses of ^{21}Ne abundances yielded CRE ages of 5.3 ± 0.9 and 5.2 ± 0.8 Myr for the Ryugu "A" and Ryugu "C" samples, respectively (Okazaki et al., 2022). By comparison, CRE ages for carbonaceous chondrites range from 2.2 to 4.5 Myr for CI chondrites (Mazor et al., 1970), 1.8–3.7 Myr for CM chondrites (Herzog et al., 1997), 5.2–5.6 Myr for CV chondrites (Scherer & Schultz, 2000), 5.0–19.2 Myr for CO chondrites (Scherer & Schultz, 2000), and 4.1 Myr for CR chondrites (Mazor

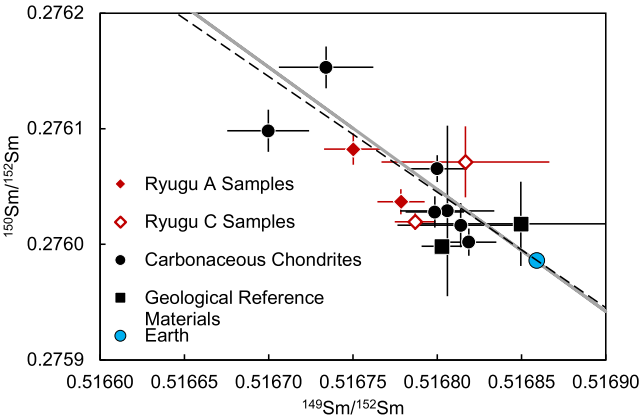

FIGURE 6. $^{150}Sm/^{152}Sm$ versus $^{149}Sm/^{152}Sm$ for the Ryugu "A" (solid red diamonds) and "C" (open red diamonds) samples, carbonaceous chondrites (black circles), and geological reference materials (black squares) measured in this study. The black dashed line is a calculated correlation line resulting from changing one atom of ^{149}Sm to ^{150}Sm. The solid gray line indicates the correlation line of lunar samples from Boyet and Carlson (2007). The blue point shows the high-precision Sm isotopic composition of the AMES Sm standard that presumably represents the Sm isotopic composition of the bulk Earth (Carlson et al., 2007). (Color figure can be viewed at wileyonlinelibrary.com)

TABLE 3. The neutron fluence (ψ) values for the samples measured here.

Sample	ψ ($\times 10^{15}$ n cm^{-2})
Meteorite samples	
Allende[a]	0.75 ± 1.34
Allende[b]	1.10 ± 0.83
Alais	4.21 ± 1.35
Orgueil	5.86 ± 1.17
Murchison	0.13 ± 0.79
Tarda	1.03 ± 0.86
Tagish Lake	0.36 ± 1.81
Ryugu samples	
Ryugu A0106	3.43 ± 0.84
Ryugu A0106-A0107	2.06 ± 0.68
Ryugu C0107	1.66 ± 0.58
Ryugu C0108	0.22 ± 2.40

[a]Allende EPL dissolution.
[b]Allende Tokyo Institute of Technology dissolution.

et al., 1970). For the carbonaceous chondrites measured here, the CI chondrites record much larger neutron fluences than the CV, CM, and C2-ungrouped chondrites, and these CI chondrite fluence values are similar to the largest Ryugu "A" sample value (Figure 6). This comparison is complicated, however, by the fact that neutron fluence depends significantly on chemical composition, and chondrites with higher H contents (e.g., CI chondrites) will have higher thermal and epithermal neutron fluence than those with lower H contents (e.g., CV chondrites). Although this could indicate similar

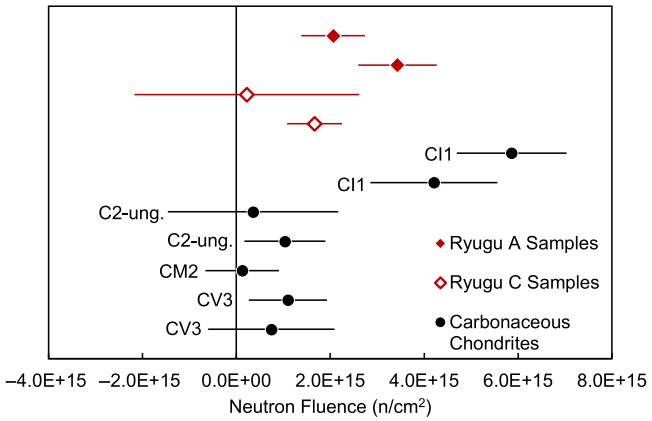

FIGURE 7. Neutron fluence (ψ) for the carbonaceous chondrites (black circles) and Ryugu "A" (solid red diamonds) and "C" (open red diamonds) samples measured in this study. (Color figure can be viewed at wileyonlinelibrary.com)

parent body origins and exposure histories of CI chondrites and Ryugu samples, a direct comparison between meteorite and Ryugu values is complicated because meteorite exposure history includes the transit time to Earth.

Using the neutron production rates within stony meteorites provided by Spergel et al. (1986), thermal neutron fluences at a depth of 2 g cm^{-2} in a body like Ryugu with percent levels of hydrogen are of order 7×10^{14} n cm^{-2} Myr^{-1} and rise with depth to $\sim 3.5 \times 10^{15}$ n cm^{-2} Myr^{-1} at 100 g cm^{-2}. Given the average neutron fluxes for Ryugu "A" samples based on the Sm data, for a near-surface sample, the calculated exposure age is 3.9 ± 2.8 Myr, overlapping the 4.1–5.3 Myr exposure ages calculated from ^{10}Be (Nishiizumi et al., 2022) and ^{21}Ne (Okazaki et al., 2022). In contrast to the suggestion from ^{10}Be data that Ryugu "C" samples contain material derived from greater depth than "A", the average neutron fluence calculated from the Sm measurements in Ryugu "C" samples is lower, though overlapping within uncertainty, of the "A" samples, whereas it should be higher if "C" samples contain material from greater depth than "A" samples. Using an expected neutron fluence from Spergel et al. (1986) at the proposed depth of 100 g cm^{-2} for "C" samples (Nishiizumi et al., 2022) leads to an exposure age of 0.3 ± 1 Myr for the average "C" samples calculated from the Sm data. Using these sample parameters, a 4 Myr exposure age at a depth of 100 g cm^{-2} would be expected to produce a $\mu^{149}Sm = 562$, much higher than measured in any Ryugu or meteorite sample studied here.

We can propose three possible explanations for the apparent difference in CRE histories calculated from ^{10}Be, ^{21}Ne, and ^{149}Sm data. Our preferred explanation is that the Ryugu samples document a relatively recent turnover of the surface of the asteroid so that the "C" samples have a lower exposure age, or an average

exposure history from shallower depths, than the "A" samples, even though the "A" samples are known to sample the current surface of Ryugu. This possibility is supported by the observation of a lack of a correlation between solar wind ^{20}Ne and cosmogenic ^{21}Ne in the Ryugu samples suggesting surface residence ages of less than a few thousand years for the "A" samples (Okazaki et al., 2022). This could also be indicative of a similar process to that seen on the Moon, where the lunar regolith is well mixed to a depth of ~100 g cm^{-2} (e.g., Curtis & Wasserburg, 1975). The second explanation notes the strong effect of H on moving the peak in neutron fluence to shallower depth (e.g., Lingenfelter et al., 1961), implying that "C" samples could derive from greater depths than this peak. The fall off, however, in neutron fluence with depth even in H-rich materials is slow enough that fluences only diminish to lower than the surface at depths over ~500 g cm^{-2} (Lingenfelter et al., 1961), much deeper than inferred for the "C" samples by any data. Third, it must be noted that the samples measured in this study are different aliquots of the materials contained in the "A" and "C" chambers of the Hayabusa2 spacecraft than the "A" and "C" samples measured in other studies. Consequently, our "C" samples may be dominated by surface material whereas the "C" samples analyzed for ^{10}Be and ^{21}Ne may contain material derived from deeper within Ryugu.

CONCLUSIONS

In this study, we report the Nd and Sm isotopic compositions of four samples of the Cb-type near-Earth asteroid (162173) Ryugu. The primary conclusions of this study are as follows:

1. The analytical techniques utilized in this study demonstrate the capability to resolve Nd and Sm isotopic anomalies in small, <20 ng sample sizes of carbonaceous chondrites and Ryugu samples via TIMS using 10^{13} Ω amplifiers.
2. Ryugu samples exhibit resolvable negative μ^{142}Nd isotopic compositions that are consistent with the values measured for carbonaceous chondrites in this study and previous studies. These results indicate that Ryugu is genetically related to the parent bodies of carbonaceous chondrites, which is in agreement with previous petrologic and isotopic studies.
3. Ryugu samples exhibit resolvable negative μ^{149}Sm isotopic compositions that are the result of exposure to galactic cosmic rays. This is demonstrated by the correlation between ^{150}Sm/^{152}Sm and ^{149}Sm/^{152}Sm ratios that fall along a calculated theoretical correlation line resulting from neutron capture on ^{149}Sm to create ^{150}Sm.
4. The calculated neutron fluence experienced by Ryugu samples is greater in the "A" samples that sample near-surface material compared to the "C" samples that may sample material from depths of 0.7–1.3 m, although the fluences overlap within uncertainty. The magnitude of ^{149}Sm deficit in "A" is consistent with an exposure age of 3.9 ± 2.8 Myr that overlaps the CRE age inferred from the ^{10}Be and ^{21}Ne data for Ryugu samples (Nishiizumi et al., 2022; Okazaki et al., 2022). The calculated neutron fluence for "C", however, is lower than, but overlapping within uncertainty, that of the "A" samples, implying either similar depths of origin for "A" and "C" samples, a lower exposure age for "C" samples, or a recent overturn in the near-surface stratigraphy of Ryugu.

Acknowledgments—This work was funded by JSPS KAKENHI grants 18H01258, 19H00715, 20H04609, and 21KK0058, and a Carnegie Postdoctoral Fellowship.

Conflict of Interest Statement—The authors declare that they have no known financial or personal conflict of interest that could have appeared to influence the work reported in this paper.

Data Availability Statement—The data that support the findings of this study are available in the supplementary material of this article.

Editorial Handling—Dr. Ingo Leya

REFERENCES

Andreasen, R., and Sharma, M. 2006. Solar Nebula Heterogeneity in p-Process Samarium and Neodymium Isotopes. *Science* 314: 806–9.

Arakawa, M., Saiki, T., Wada, K., Ogawa, K., Kadono, T., Shirai, K., Sawada, H., et al. 2020. An Artificial Impact on the Asteroid (162173) Ryugu Formed a Crater in the Gravity-Dominated Regime. *Science* 368: 67–71.

Bouvier, A., and Boyet, M. 2016. Primitive Solar System Materials and Earth Share a Common Initial ^{142}Nd Abundance. *Nature* 537: 399–402.

Bouvier, A., Vervoort, J. D., and Patchett, P. J. 2008. The Lu-Hf and Sm-Nd Isotopic Composition of CHUR: Constraints from Unequilibrated Chondrites and Implications for the Bulk Composition of Terrestrial Planets. *Earth and Planetary Science Letters* 273: 48–57.

Boyet, M., Bouvier, A., Frossard, P., Hammouda, T., Garçon, M., and Gannoun, A. 2018. Enstatite Chondrites EL3 as Building Blocks for the Earth: The Debate over the ^{146}Sm–^{142}Nd Systematics. *Earth and Planetary Science Letters* 488: 68–78.

Boyet, M., and Carlson, R. W. 2005. ^{142}Nd Evidence for Early (>4.53 Ga) Global Differentiation of the Silicate Earth. *Science* 309: 576–581.

Boyet, M., and Carlson, R. W. 2007. A Highly Depleted Moon or a Non-Magma Ocean Origin for the Lunar Crust? *Earth and Planetary Science Letters* 262: 505–516.

Brennecka, G. A., Borg, L. E., and Wadhwa, M. 2013. Evidence for Supernova Injection into the Solar Nebula and the Decoupling of r-Process Nucleosynthesis. *Proceedings of the National Academy of Sciences of the United States of America* 110: 17241–46.

Burkhardt, C., Borg, L. E., Brennecka, G. A., Shollenberger, Q. R., Dauphas, N., and Kleine, T. 2016. A Nucleosynthetic Origin for the Earth's Anomalous ^{142}Nd Composition. *Nature* 537: 394–98.

Carlson, R. W., Boyet, M., and Horan, M. 2007. Chondrite Barium, Neodymium, and Samarium Isotopic Heterogeneity and Early Earth Differentiation. *Science* 316: 1175–78.

Curtis, D. B., and Wasserburg, G. J. 1975. Apollo 17 Neutron Stratigraphy: Sedimentation and Mixing in the Lunar Regolith. *The Moon* 13: 185–227.

Eugster, O., Herzog, G., Marti, K., and Caffee, M. 2006. Irradiation Records, Cosmic-Ray Exposure Ages, and Transfer Times of Meteorites. In *Meteorites and the Early Solar System II*, edited by D. S. Lauretta, and H. Y. McSween, 829–851. Tucson, AZ: University of Arizona Press.

Frossard, P., Israel, C., Bouvier, A., and Boyet, M. 2022. Earth's Composition was Modified by Collisional Erosion. *Science* 377: 1529–32.

Fukai, R., and Yokoyama, T. 2017. Neodymium Isotope Heterogeneity of Ordinary and Carbonaceous Chondrites and the Origin of Non-Chondritic ^{142}Nd Compositions in the Earth. *Earth and Planetary Science Letters* 474: 206–214.

Fukai, R., and Yokoyama, T. 2019. Nucleosynthetic Sr–Nd Isotope Correlations in Chondrites: Evidence for Nebular Thermal Processing and Dust Transportation in the Early Solar System. *The Astrophysical Journal* 879: 79.

Gannoun, A., Boyet, M., Rizo, H., and El Goresy, A. 2011. ^{146}Sm-^{142}Nd Systematics Measured in Enstatite Chondrites Reveals a Heterogeneous Distribution of ^{142}Nd in the Solar Nebula. *Proceedings of the National Academy of Sciences of the United States of America* 108: 7693–97.

Garçon, M., Boyet, M., Carlson, R. W., Horan, M. F., Auclair, D., and Mock, T. D. 2018. Factors Influencing the Precision and Accuracy of Nd Isotope Measurements by Thermal Ionization Mass Spectrometry. *Chemical Geology* 476: 493–514.

Grott, M., Knollenberg, J., Hamm, M., Ogawa, K., Jaumann, R., Otto, K., Delbo, M., et al. 2019. Low Thermal Conductivity Boulder with High Porosity Identified on C-Type Asteroid (162173) Ryugu. *Nature Astronomy* 3: 971–76.

Herzog, G. F., Vogt, S., Albrecht, A., Xue, S., Fink, D., Klein, J., Middleton, R., Weber, H. W., and Schultz, L. 1997. Complex Exposure Histories for Meteorites with "Short" Exposure Ages. *Meteoritics & Planetary Science* 32: 413–422.

Hidaka, H., Ebihara, M., and Yoneda, S. 2000. Isotopic Study of Neutron Capture Effects on Sm and Gd in Chondrites. *Earth and Planetary Science Letters* 180: 29–37.

Hidaka, H., Sakuma, K., Nishiizumi, K., and Yoneda, S. 2017. Isotopic Evidence for Multi-Stage Cosmic-Ray Exposure Histories of Lunar Meteorites: Long Residence on the Moon and Short Transition to Earth. *The Astronomical Journal* 153: 274 (7 pp).

Hidaka, H., Yoneda, S., and Nishiizumi, K. 2009. Cosmic-Ray Exposure Histories of Martian Meteorites Studied from Neutron Capture Reactions of Sm and Gd Isotopes. *Earth and Planetary Science Letters* 288: 564–571.

Hopp, T., Dauphas, N., Abe, Y., Aléon, J., Alexander, C. M. O'D., Amari, S., Amelin, Y., et al. 2022. Ryugu's Nucleosynthetic Heritage from the Outskirts of the Solar System. *Science Advances* 8: eadd8141.

Jochum, K. P., Weis, U., Schwager, B., Stoll, B., Wilson, S. A., Haug, G. H., Andreae, M. O., and Enzweiler, J. 2016. Reference Values Following ISO Guidelines for Frequently Requested Rock Reference Materials. *Geostandards and Geoanalytical Research* 40: 333–350.

Johnston, S., Brandon, A., McLeod, C., Rankenburg, K., Becker, H., and Copeland, P. 2022. Nd Isotope Variation Between the Earth–Moon System and Enstatite Chondrites. *Nature* 611: 7–9.

Kagami, S., and Yokoyama, T. 2016. Chemical Separation of Nd from Geological Samples for Chronological Studies Using ^{146}Sm/^{142}Nd and ^{147}Sm/^{143}Nd Systematics. *Analytica Chimica Acta* 937: 151–59.

Kawasaki, N., Nagashima, K., Sakamoto, N., Matsumoto, T., Bajo, K. I., Wada, S., Igami, Y., et al. 2022. Oxygen Isotopes of Anhydrous Primary Minerals show Kinship between Asteroid Ryugu and Comet 81P/Wild2. *Science Advances* 8: eade2067.

Kitazato, K., Milliken, R. E., Iwata, T., Abe, M., Ohtake, M., Matsuura, S., Arai, T., et al. 2019. The Surface Composition of Asteroid 162173 Ryugu from Hayabusa2 Near-Infrared Spectroscopy. *Science* 364: 272–75.

Leya, I., Lange, H.-L., Neumann, S., Wieler, R., and Michell, R. 2000. The Production of Cosmogenic Nuclides in Stony Meteoroids by Galactic Cosmic-Ray Particles. *Meteoritics & Planetary Science* 35: 259–286.

Lingenfelter, R. E., Canfield, E. H., and Hampel, V. E. 1972. The Lunar Neutron Flux Revisited. *Earth and Planetary Science Letters* 16: 355–369.

Lingenfelter, R. E., Canfield, E. H., and Hess, W. N. 1961. The Lunar Neutron Flux. *Journal of Geophysical Research* 66: 2665–71.

Lugmair, G. W., and Marti, K. 1977. Sm-Nd-Pu Timepieces in the Angre Dos Reis Meteorite. *Earth and Planetary Science Letters* 35: 273–284.

Mazor, E., Heymann, D., and Anders, E. 1970. Noble Gases in Carbonaceous Chondrites. *Geochimica et Cosmochimica Acta* 34: 781–824.

McCain, K. A., Matsuda, N., Liu, M.-C., McKeegan, K. D., Yamaguchi, A., Kimura, M., Tomioka, N., et al. 2023. Early Fluid Activity on Ryugu Inferred by Isotopic Analyses of Carbonates and Magnetite. *Nature Astronomy* 7: 1–9.

Moynier, F., Dai, W., Yokoyama, T., Hu, Y., Paquet, M., Abe, Y., Aléon, J., et al. 2022. The Solar System Calcium Isotopic Composition Inferred from Ryugu Samples. *Geochemical Perspectives Letters* 24: 1–6.

Mughabghab, S. F. 1984. *Neutron Cross Sections Volume 1: Neutron Resonance Parameters and Thermal Cross Sections*. Cambridge: Academic Press.

Nakamura, T., Matsumoto, M., Amano, K., Enokido, Y., Zolensky, M. E., Mikouchi, T., Genda, H., et al. 2022. Formation and Evolution of Carbonaceous Asteroid Ryugu: Direct Evidence from Returned Samples. *Science* 379: eabn8671.

Nishiizumi, K., Caffee, M. W., Nagao, K., Masarik, J., Okazaki, R., Yurimoto, H., Nakamura, T., et al. 2022.

Exposure Conditions of Samples Collected on Ryugu's Two Touchdown Sites Determined by Cosmogenic Nuclides ^{10}Be and ^{26}Al. 53rd Lunar and Planetary Science Conference, abstract #1777.

Okada, T., Fukuhara, T., Tanaka, S., Taguchi, M., Arai, T., Senshu, H., Sakatani, N., et al. 2020. Highly Porous Nature of a Primitive Asteroid Revealed by Thermal Imaging. *Nature* 579: 518–522.

Okazaki, R., Marty, B., Busemann, H., Hashizume, K., Gilmour, J. D., Meshik, A., Kitajima, F., et al. 2022. Noble Gases and Nitrogen in Samples of Asteroid Ryugu Record its Volatile Sources and Recent Surface Evolution. *Science* 379: eabo0431.

Paquet, M., Moynier, F., Yokoyama, T., Dai, W., Hu, Y., Abe, Y., Aléon, J., et al. 2022. Contribution of Ryugu-Like Material to Earth's Volatile Inventory by Cu and Zn Isotopic Analysis. *Nature Astronomy* 7: 182–89.

Qin, L., Carlson, R. W., and Alexander, C. M. O'D. 2011. Correlated Nucleosynthetic Isotopic Variability in Cr, Sr, Ba, Sm, Nd and Hf in Murchison and QUE 97008. *Geochimica et Cosmochimica Acta* 75: 7806–28.

Render, J., and Brennecka, G. A. 2021. Isotopic Signatures as Tools to Reconstruct the Primordial Architecture of the Solar System. *Earth and Planetary Science Letters* 555: 116705.

Russ, G. P., Burnett, D. S., Lingenfelter, R. E., and Wasserburg, G. J. 1971. Neutron Capture on ^{149}Sm in Lunar Samples. *Earth and Planetary Science Letters* 13: 53–60.

Saji, N. S., Wielandt, D., Holst, J. C., and Bizzarro, M. 2020. Solar System Nd Isotope Heterogeneity: Insights into Nucleosynthetic Components and Protoplanetary Disk Evolution. *Geochimica et Cosmochimica Acta* 281: 135–148.

Sanborn, M. E., Carlson, R. W., and Wadhwa, M. 2015. ^{147,146}Sm–^{143,142}Nd, ^{176}Lu–^{176}Hf, and ^{87}Rb–^{87}Sr Systematics in the Angrites: Implications for Chronology and Processes on the Angrite Parent Body. *Geochimica et Cosmochimica Acta* 171: 80–99.

Scherer, P., and Schultz, L. 2000. Noble Gas Record, Collisional History, and Pairing of CV, CO, CK, and Other Carbonaceous Chondrites. *Meteoritics & Planetary Science* 35: 145–153.

Shollenberger, Q. R., Borg, L. E., Render, J., Ebert, S., Bischoff, A., Russell, S. S., and Brennecka, G. A. 2018. Isotopic Coherence of Refractory Inclusions from CV and CK Meteorites: Evidence from Multiple Isotope Systems. *Geochimica et Cosmochimica Acta* 228: 62–80.

Spergel, M. S., Reedy, R. C., Lazareth, O. W., Levy, P. W., and Slatest, L. A. 1986. Cosmogenic Neutron-Capture-Produced Nuclides in Stony Meteorites. *Journal of Geophysical Research* 91: 483–494.

Sugita, S., Honda, R., Morota, T., Kameda, S., Sawada, H., Tatsumi, E., Yamada, M., et al. 2019. The Geomorphology, Color, and Thermal Properties of Ryugu: Implications for Parent-Body Processes. *Science* 364: p.eaaw0422.

Tachibana, S., Sawada, H., Okazaki, R., Takano, Y., Sakamoto, K., Miura, Y. N., Okamoto, C., et al. 2022. Pebbles and Sand on Asteroid (162173) Ryugu: In Situ Observation and Particles Returned to Earth. *Science* 375: 1011–16.

Takaki, N., Cho, Y., Morota, T., Tatsumi, E., Honda, R., Kameda, S., Yokota, Y., et al. 2022. Resurfacing Processes Constrained by Crater Distribution on Ryugu. *Icarus* 377: 114911.

Wang D. and Carlson R. W. (2022) Tandem-Column Extraction Chromatography for Nd Separation: Minimizing Mass-Independent Isotope Fractionation for Ultrahigh-Precision Nd

Yokoyama, T., Nagashima, K., Nakai, I., Young, E. D., Abe, Y., Aléon, J., Alexander, C. M. O'D., et al. 2023. Samples Returned from the Asteroid Ryugu are Similar to Ivuna-Type Carbonaceous Meteorites. *Science* 379: eabn7850.

SUPPORTING INFORMATION

Additional supporting information may be found in the online version of this article.

Table S1.